The HKU Scholars Hub   The University of Hong Kong   香港大學學術庫

Title	**Anomalous diffusivity and electric conductivity for low concentration electrolytes in nanopores**
Author(s)	**Lai, SK; Kau, CY; Tang, YW; Chan, KY**
Citation	**Physical Review E - Statistical, Nonlinear, And Soft Matter Physics, 2004, v. 69 n. 5 2, p. 051203-1-051203-12**
Issued Date	**2004**
URL	**http://hdl.handle.net/10722/42637**
Rights	**Physical Review E (Statistical, Nonlinear, and Soft Matter Physics). Copyright © American Physical Society.**

Anomalous diffusivity and electric conductivity for low concentration electrolytes in nanopores

S. K. Lai[1,*] and C. Y. Kau[1]

[1]*Complex Liquids Laboratory, Department of Physics, National Central University, Chung-li, Taiwan, Republic of China*

Y. W. Tang[2] and K. Y. Chan[2]

[2]*Department of Chemistry, The University of Hong Kong, Pokfulam Road, Hong Kong S.A.R., China*

We apply equilibrium and nonequilibrium molecular dynamics simulations to study the dynamic properties of electrolytes in nanopores. The realistic primitive model and the restrictive primitive model widely used in the statistical mechanics of liquid-state theory are applied to model the electrolytes. The electrolytic ions are immersed in water, treated in this work as either a dielectric continuum ignoring the size of solvent molecules or a macroscopic dielectric continuum (polar property) plus neutral soft spheres, and the aqueous electrolyte is put in a confined space. To simulate a condition mimicking closely processes of practical interest and yet maintaining the simulation computationally manageable, we consider an infinitely long and uncharged cylindrical tube. The equilibrium property of the self-diffusion coefficent D and the nonequilibrium property of electric conductivity σ are computed in terms of electrolyte concentration, particle size, and cylindrical pore radius. The simulation results for the continuum solvent restrictive primitive model and continuum solvent primitive model show normal behavior for D versus pore radius R at ionic concentration $0.1M$—i.e., D decreases with decreasing R—display an R independence of D at a certain threshold concentration and undergo an anomalous increase in D with reducing R at a lower value $0.025M$. The mechanism of the anomaly at the ionic concentration $0.025M$ was sought for and interpreted in this work to arise from the energetic and entropic factors. Our simulated data of σ at this same concentration follow the same trend as D. To delve further into the transport properties, we perform simulation studies for the discrete solvent primitive model and make a detailed analysis of the characteristic of the ion radial density functions. Comparison of the latter functions with those in the continuum solvent primitive model sheds light on the simulated diffusion coefficient within the context of discrete solvent primitive model which is about two orders of magnitude less. This difference in D is naturally attributed to the solvent effect. Similar disparities were reported by others for the discrete and continuum restrictive primitive models.

PACS number(s): 66.10.−x

I. INTRODUCTION

Electrolytes in a confined space, nanopores in particular, resemble many physical systems encountered in our daily life. Recently, studies of this spatially restricted system have attracted a great deal of attention, both experimentally and theoretically. One possible impetus for the intensified research activities may be due to the marvellous discovery of the crystal structure of bacterial potassium channels [1]. The latter can serve as a prototype example in studies of the structures of voltage-gated channels. In this regard, ion channels belong to one of these many systems. The understanding of ions in a confined geometry in a state of either equilibrium or nonequilibrium is important in biological processes. Well known cases are the numerical studies of biological channels which have demonstrated specific ion selectivity phenomenon, but the same energetic consideration is found to be intact for simulations of ionic flow in the aqueous baths outside the channels. The high rate of ionic transport is thus a distinct feature observed in pores. In the area of material science and a somewhat closely related area, electrochemistry, interest in the properties of confined electrolytes has been directed to finding an optimized performance of fuel cells that depend on Nafion membranes and porous electrodes.

During the past two decades, computer simulations have been used to study the static and dynamic properties of molecules or ions in porous media [2–7]. These simulation studies are mainly devoted to an understanding of the equilibrium properties of the structures of channels and of the energetic and dynamics of aqueous dilute electrolytes in them. In most simulation studies, such as the electrolytes adsorption, the ions are treated within the primitive model (PM) and the solvent is approximated by a continuum dielectric constant background. The papers of Rivera and Sorenson [8], Lee and Chan [9], Boda *et al.* [10], and Hribar *et al.* [11] are a few representatives of these recent works. In addition, simulations of electrolytes in nanopores that aim at a more realistic molecular model of solvent, the so-called discrete solvent restrictive primitive model, have been proposed also. [12,13] Concurrently, there are other simulation attempts [4–7] that give proper attention to the behavior of molecules in molecular sieves. Here effort is directed to classify the diffusion modes into normal (or tracer) and single-file diffusions. This kind of simulation studies of molecular diffusion can shed considerable light on the underlying mechanism of phase separation for particles in restricted space [6]. While these simulation works have uncovered such anomalies as the charge non-neutrality [9], salt exclusion [14], selective

---

*Corresponding author.

adsorption [12], attractive double-layer forces [10], dual-mode diffusion [6], etc., relatively fewer works are reported for the transport properties of confined electrolytes despite the fact that they are of greater industrial importance.

Transport properties of electrolytes in restricted space have been motivated greatly by experiments. Steck and Yeager [15] and Gavach *et al.* [16] carried out one of the early conductivity experiments in perfluorosulfonic acid membranes by means of an ac impedance method. Lack of a definitive measurement of membrane pore sizes and the poor characterization of the membrane structure have made the interpretation of electric conductivity results extremely difficult. Electrical conductivity measurements with various electrolytes in track-etched mica membranes and the conductance through a single submicrometer diameter pore using a scanning ion-conductance microscope have been reported by Westerman-Clark and Anderson [17] and Hansma *et al.* [18], respectively. We should perhaps mention the patch-clamp technique which has been widely applied to determine the current-voltage characteristics of various biological channels in different electrolytic environment [19]. Since the aforementioned techniques are generally difficult for pores of a few nanometers, there remain ambiguities in the interpretation of experimental data obtained. Under this circumstance, the molecular dynamics (MD) method is an indispensable tool for it can stretch into the regime inaccessible to experiments. Lynden-Bell and Rasaiah [20] performed an equilibrium MD simulation for a sample comprising one solute molecule and water molecules in an infinite cylindrical pore with smooth repulsive walls. The solvent is treated there as pointlike molecules (the SPC/E model) and channels of various sizes are assumed uncharged. In the following years, equilibrium MD (EMD) simulations were applied [21,22] to study more realistic biological ion channels. While it is possible, in principle, to perform a long-time simulation and compare the results with, say, the patch-clamp experimental data, in practice it is still numerically tedious to do long-time MD simulation for atomic channels.

For the study of D and σ of interest here, we may, however, proceed as follows. First, we apply the EMD simulation to obtain short-time diffusion coefficients. Using the latter, we predict the current in a nonequilibrium situation within the context of the Nernst-Planck theory of ionic flux and determine the ionic conductivity by the Nernst-Einstein theory [23,24]. Then we carry out a nonequilibrium MD (NEMD) simulation and check the results against the EMD-projected conductivity based on the Nernst-Einstein theory. With this strategy in mind, our plan in this work is to apply the EMD and NEMD simulations to electrolytes and study the mobility of ions in an infinitely long, uncharged cylindrical nanopore within which contains the solvent which is modeled as (i) a continuum dielectric constant ignoring the size of ions and (ii) a continuum dielectric constant simulating the polar property plus a collection of neutral soft spheres reflecting its molecular nature. Differing from our preceding works [13,25] where we used the restrictive primitive model and fixed the electrolytic concentration at $0.1M$, we consider here different sizes for the sodium and chlorine ions (the realistic primitive model) and extend the simulation to lower electrolytic concentrations. The due consideration of

size disparity for cations and anions is reminiscent of the normal, single-file, and dual-mode diffusions numerically predicted for a binary adsorbate mixture in AlPO$_4$-5. These simulation studies of molecular diffusion were motivated mainly by experiments [5,26–28] reported to have observed either normal or single-file diffusion for the single adsorbed species in AlPO$_4-5$ zeolite. These diffusion behaviors were interpreted recently by Sholl and Fichthorn [6] who proposed a generalized geometric criterion. It would be instructive to see the bearing of this criterion against our realistic primitive model. We found that D decreases with decreasing pore radius at ionic concentration $0.1M$, displays a near R independence of D at a certain threshold concentration and shows an anomalous increment with decreasing R at concentration $0.025M$. The simulated σ carried out at the electrolytic concentration $0.025M$ is consistent with this D anomaly. To be explained below, we attribute this anomaly to competitive contributions between the energetic and entropic factors.

II. MOLECULAR DYNAMICS SIMULATION

In this section, we present details of the EMD and NEMD simulations applied to study dynamic properties of electrolytes in confined space.

A. Interparticle potential

In both the equilibrium and nonequilibrium MD simulations, we need, first of all, an interparticle potential function. To construct this function generally and to set up the simulation environment, we proceed as follows. First, the *molecular* behavior of the solvent is approximated by a system of neutral soft spheres and its polar property, comprising the molecular multipoles and hydrogen bonding, is reflected in the reduction of the interactions between ions by a factor $1/\varepsilon_r$ where ε_r is a dielectric constant simulating a *macroscopic* continuum background. We use the primitive model for electrolytic ions, but treat their short-range interaction as soft cores. The ion-ion, ion-solvent, and solvent-solvent interactions are modeled separately by a soft core Week-Chandler-Anderson potential given by

$$u_{\lambda\mu}^{\text{soft}}(r_{ij}) = \begin{cases} u_{LJ}(r_{ij}) + \epsilon_{\lambda\mu}, & r_{ij} \leqslant r_{\min}(\lambda\mu), \\ 0 & \text{otherwise}, \end{cases} \quad (1)$$

where

$$u_{LJ}(r_{ij}) = 4\epsilon_{\lambda\mu}\left[\left(\frac{d_{\lambda\mu}}{r_{ij}}\right)^{12} - \left(\frac{d_{\lambda\mu}}{r_{ij}}\right)^{6}\right] \quad (2)$$

is the Lennard-Jones (LJ) potential. The λ or μ in Eq. (1) denotes anion, cation, or solvent, $\epsilon_{\lambda\mu}$ and $d_{\lambda\mu}$ are the LJ energy and the soft-sphere diameter parameters of the particle-particle (which can be anion-anion, cation-cation, anion-cation, anion- or cation-solvent, or solvent-solvent), and $r_{\min}(\lambda\mu)=2^{1/6}d_{\lambda\mu}$ is the location of the minimum of the untruncated LJ potential. To account for the long-range Coulomb tail of ions, we correct the soft-core part by the electrostatic interaction in a continuum solvent as
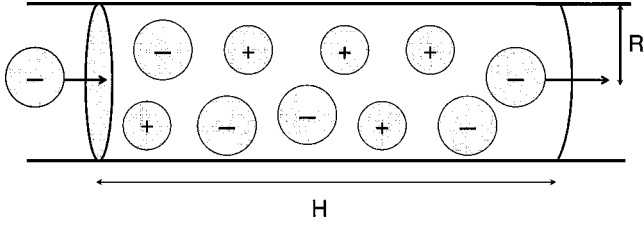
FIG. 1. Schematic figure for the cylindrical cell with periodic boundary condition in the axial direction. Different sizes for anions and cations emphasize the realistic primitive model.

$$u_{\lambda\mu}^{C}(r_{ij}) = \frac{q_i q_j}{4\pi\epsilon_0\epsilon_r r_{ij}}. \tag{3}$$

Here q_i is the charge of the ith ion and ϵ_0 is the dielectric permittivity of the vacuum. In this work, we consider two specific cases of interest for the interaction potential. The first case only accounts for the soft-core interactions among ions ignoring those counterparts of the solvent molecules. The total interaction potential is

$$u_{\lambda\mu}^{CPM} = \tilde{u}_{\lambda\mu}^{soft} + u_{\lambda\mu}^{C}, \tag{4}$$

where $\tilde{u}_{\lambda\mu}^{soft}$ is $u_{\lambda\mu}^{soft}$ with the index λ or μ takes on *only* anions or cations. We refer to Eq. (4) as the *continuum* solvent approximation. For the second case, the long-range interactions between anions and cations are again given by Eq. (3), but, in addition, the cation-solvent, anion-solvent, and solvent-solvent interactions are assumed to take on the same potential form as Eq. (1). Within this so-called *discrete* solvent primitive model (DSPM), we have

$$u_{\lambda\mu}^{DPM} = u_{\lambda\mu}^{soft} + u_{\lambda\mu}^{C}. \tag{5}$$

Note that the index λ or μ in $u_{\lambda\mu}^{soft}$ now runs over the anion, cation, or neutral solvent molecule and in contrast to $u_{\lambda\mu}^{C}$ where the λ or μ takes on an anion or cation only. Equations (1)–(5) are basic functions to be used in the MD simulation below. To proceed to numerical simulation, we place all the particles inside a cylindrical cell of radius R and length H (Fig. 1). A periodic boundary condition is applied along the axial direction denoted by z. Now the confinement of particles within the cylindrical cell means that we need to account for the ion/solvent-wall interactions. For an uncharged channel, we use the analytical formula derived previously by Tjatjopoulous *et al.* [29] In their work Tjatjopoulous *et al.* considered micropores of a circular as well as a polygonal cross sections. In the present work, only the cylindrical channel is studied. Explicitly, the particle-wall potential is given by

$$u_{\lambda w}(r_i) = \begin{cases} u_{LJ,\lambda w}(r_i) + u_{LJ,\lambda w}(r_{\min}(\lambda w)), & r_i \geq r_{\min}(\lambda w), \\ 0, & \text{otherwise,} \end{cases} \tag{6}$$

in which

TABLE I. Lennard-Jones distance and energy parameters for the restrictive primitive models (Na$^+$,Na$^-$) and (Cl$^+$,Cl$^-$), primitive model (Na$^+$,Cl$^-$), ion-solvent and ion-wall interactions. The solvent when treated on a molecular level is characterized by oxygen O. The ion-wall (W) Lennard-Jones parameters are calculated by the Lorentz-Berthelot rule.

$\lambda\mu$	$d_{\lambda\mu}$ (10^{-10} m)	$\epsilon_{\lambda\mu}$ (10^{-23} J)
Na-Na	2.73	59.37
Cl-Cl	4.86	27.87
Na-Cl	3.87	28.32
O-O	3.169	107.95
Na-O	2.876	86.6
Cl-O	3.25	86.6
W-W	3.87	28.32
Na-W	3.30	41.00
Cl-W	4.37	28.09
O-W	3.52	55.29

$$u_{LJ,\lambda w}(r_i) = n_w\epsilon_{\lambda w}\pi^2\left(\frac{63}{32}\frac{F(-9/2,-9/2,1;(r_i/R)^2)}{(R/d_{\lambda w} - r_i/d_{\lambda w})^{10}[(R+r_i)/R]^{10}}\right.$$
$$\left. - \frac{3F(-3/2,-3/2,1;(r_i/R)^2)}{(R/d_{\lambda w} - r_i/d_{\lambda w})^4[(R+r_i)/R]^4}\right) \tag{7}$$

is the shifted LJ-type wall potential. In the above, n_w is the reduced surface number density of the wall, $d_{\lambda w}$ and $\epsilon_{\lambda w}$ are the distance and energy parameters for the particle-wall interaction, r_i is the radial distance of the ith particle from the center of the cylinder, $r_{\min}(\lambda w)$ is the location of the minimum of the LJ particle-wall potential (unless specified, the word "particle" is hereafter referred to generally as anions, cations, or solvent molecules), and $F(a,b,c;x)$ is the hypergeometric function. Note that we assume the dielectric properties of the wall and outside are the same as the solvent in appealing to Eq. (6) for the particle-wall interaction. Such a judicious assumption avoids the complication to account for the boundary condition arising from different dielectric media. Given Eqs. (1)–(6) for the particle interaction potential, both EMD and NEMD simulations can be carried out if the particle LJ parameters are available. In this work, we have adopted the same set of LJ parameters previously used by Spohr [30] and more recently by Crozier *et al.* [31] to model the electrolyte Na$^+$, Cl$^-$, and water molecules. As for the particle-wall LJ parameters, they are calculated according to the Lorentz-Berthelot rule. [32] We record all these LJ parameters in Table I.

B. Equilibrium MD simulation

We shall use *NVT* ensemble in our EMD simulation. The system, confined within volume V, consists of N particles, which is the total number of either anions, cations, and solvent molecules for the *discrete* solvent primitive model or only anions plus cations for the *continuum* solvent primitive model. These particles are thermally maintained at room temperature, which is technically fixed by the Gaussian ther-

TABLE II. Reduced units (see text) used in the simulation. The anions or cations are maintained at temperature 298.15 K in both the RPM (first and second rows) and PM (third row). The τ used in the simulation is 10^{-15} s.

RPM or PM	$m_{\lambda\mu}$ (a.u.)	ρ^*/ρ (10^{-29} m³)	T^*/T (K^{-1})	τ^*/τ (10^{10} s^{-1})	D^*/D (10^7 s m^{-2})	σ^*/σ (10^{-5} Ωm)
(Na$^+$,Na$^-$)	23	2.0346	0.02324	45.662	2.93858	1.3866
(C$^+$,Cl$^-$)	35	11.4791	0.04952	14.244	2.97194	3.7041
(Na$^+$,Cl$^-$)	29	5.7961	0.04873	19.812	3.37010	2.1608

mostat [33]. The axial self-diffusion coefficient of the λ-type species of particles, D_λ, was calculated according to the Einstein formula (dropping the index for particles)

$$D_\lambda = \frac{1}{2}\lim_{t\to\infty}\langle|z_\lambda(t) - z_\lambda(0)|^2\rangle/t, \qquad (8)$$

where the brackets $\langle\cdots\rangle$ denote the ensemble average of the mean-square axial displacement of the λ-type species. Strictly speaking, mutual diffusion coefficients should be considered especially in the DSPM which consists of a mixture of three different species. MacElroy and Suh [34] have proposed a means to compute the diffusion coefficients in a mixture and relate them to individual fluxes. Since the concentration of ions of interest here ($\leq 0.1M$) is dilute, we may comfortably apply Eq. (8) only and use it to compute the self-diffusion coefficient of ions. At this point, we should mention several technical details used in the simulation. First, the equations of motion that yield the positions of particles were here solved numerically by the modified Verlet algorithm [35]. Since the particles are restricted to move in an infinite cylindrical cell, the method of the periodic boundary condition along the z axis is imposed. The methodology proposed by Rapaport [36] is sufficient for this purpose. Second, for convenience in simulation, we adopt reduced units. In terms of mass m_λ, distance parameter $d_{\lambda\mu}$, and energy parameter $\epsilon_{\lambda\mu}$, the reduced units are defined for temperature $T^* = k_B T/\epsilon_{\lambda u}$, time step $\tau^* = \tau[\epsilon_{\lambda\mu}/(m_\lambda d_{\lambda\mu}^2)]^{1/2}$, density $\rho^* = (N/V)d_{\lambda\mu}^3$, and finally self-diffusion coefficient $D^* = D/(\epsilon_{\lambda\mu}d_{\lambda\mu}^2/m_\lambda)^{1/2}$. For convenience in conversion, we give in Table II details of these reduced quantities applied to cases of interest.

C. Nonequilibrium MD simulations

For NEMD, we study the transport property of an electrolyte in a nanotube focusing in particular the electric flow of ions. Instead of using the dual-control-volume grand canonical MD [37] technique supposedly more suit to studying the mobility of ions, here we follow Tang *et al.* [25] and others [38], adopting the method of an electric potential gradient. This approach has the advantage of easy implementation and computationally it requires lesser amount of computing time in comparison with the former method. The electric potential gradient method, as the name indicates, amounts to applying (axially) a constant uniform electric field E_z to the cylindrical channel. In response to the E_z, the anions and cations, on the average, move in opposite directions over a time period. In the course of the motion of ions, a constant ion concentration

is maintained in the simulation cell by the axial periodic boundary condition. This method resembles the artificial color current method [39] used in the NEMD simulation of the transport properties of non-Coulombic systems. In calculating the conductivity, the external electric field will generate Ohmic heat. This unavoidable feature will raise the temperature of the system. In this work, we keep a constant temperature by employing the method proposed by Evans and Morris [40] as follows. Writing the induced axial current density as J_z, the non-Newtonian equations of motion are

$$\frac{d}{dt}\mathbf{r}_i = \mathbf{p}_i/m \qquad (9)$$

and

$$\frac{d}{dt}\mathbf{p}_i = \mathbf{F}_i + q_i E_z \hat{\mathbf{e}}_z - \zeta\left(\mathbf{p}_i - \frac{mVq_iJ_z}{q_i^2N}\hat{\mathbf{e}}_z\right), \qquad (10)$$

where $\mathbf{r}_i$, $\mathbf{p}_i$, and $\mathbf{F}_i$ are the position, momentum, and force vectors of the ith particle, respectively, ζ is the Gaussian thermostat parameter, and $J_z = [\sum_{i=1}^N q_i v_{i,z}]/V$, where $v_{i,z}$ is the axial velocity. Since the PM takes into consideration the size disparity for cations and anions, we use $J_z = [\sum_{i=1}^{N+} q_{+,i} v_{+,i,z}]/V_+ + [\sum_{i=1}^{N-} q_{-,i} v_{-,i,z}]/V_-$ for the current density of the PM. The detailed functional forms of ζ as well as that of T in the context of Gaussian constraint equation are given in Tang *et al.* [25]. Finally, the conductivity can be obtained as

$$\sigma = \lim_{E_z\to 0} J_z/E_z. \qquad (11)$$

In accordance with the reduced units introduced above, the current density, electric field strength, and electric conductivity are given by $J_z^* = [(m_\lambda d_{\lambda\mu}^6)/(e^2\epsilon_{\lambda\mu})]^{1/2}J_z$, $E_z^* = (d_{\lambda\mu}e/\epsilon_{\lambda\mu})E_z$, and $\sigma^* = [(m_\lambda d_{\lambda\mu}^4\epsilon_{\lambda\mu})^{1/2}/e^2]\sigma$, respectively. For the convenience of the reader, values of the reduced units are collected in Table II also.

III. NUMERICAL RESULTS

We present numerical data for the self-diffusion coefficient and electric conductivity first for the continuum solvent restrictive primitive model (CSRPM) and then for the continuum solvent primitive model (CSPM). The simulation results that emphasize the effects of molecular behavior of water within the DSPM for the same equilibrium quantities are also presented in this section.
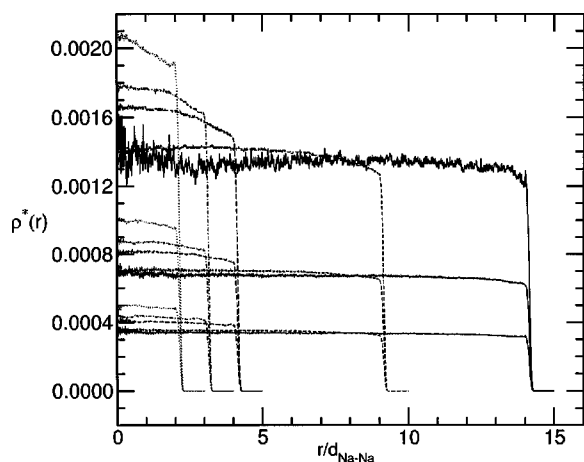
FIG. 2. Ionic radial density function $\rho^*_{Na}(r)=[N_{Na^+}(r)$ $+N_{Na^-}(r)]d^3_{Na\text{-}Na}/V$, r being the radial distance from the cylindrical axis, for continuum solvent RPM:(Na$^+$,Na$^-$) evaluated by taking the time average of $2\times10^7\tau^*$ for $R/d_{Na\text{-}Na}=3$ (dotted line), 4 (dot-dashed line), 5 (long-dashed line), 10 (short-dashed line), and 15 (solid line) at $c_{Na}=0.1M$ (top), $0.05M$ (middle) and $0.025M$ (bottom). The total number of anions and cations is 228 and $d_{Na\text{-}Na}$ $=2.73$ Å.

A. Self-diffusion coefficient: Continuum solvent RPM vs continuum solvent PM

We begin by pointing out a consequence arising from the ion-wall interaction. For concreteness, we plot in Figs. 2 and 3 the radial density profiles $\rho^*(r)=[N_{\lambda+}(r)+N_{\lambda-}(r)]d^3_{\lambda\lambda}/V$ of the RPM sodium, $\lambda=Na$, and chlorine, $\lambda=Cl$, respectively. The ionic concentrations defined by $c_\lambda=N_{\lambda+}/V=N_{\lambda-}/V$ $=0.025M$, $0.05M$ and $0.1M$ are considered for each of the RPM systems. These figures reveal two interesting features. The first feature is that the RPM sodium $\rho^*(r)$ confined to the channel of radius $R=3d_{Na\text{-}Na}$ at $c_{Na}=0.1M$ *maximizes* near the axis of the cylinder and decreases linearly with the radial distance toward the cylindrical wall, whereas for the RPM chlorine at the same R and c_{Cl}, $\rho^*(r)$ *minimizes* near the cylindrical center and increases linearly with the radial dis-
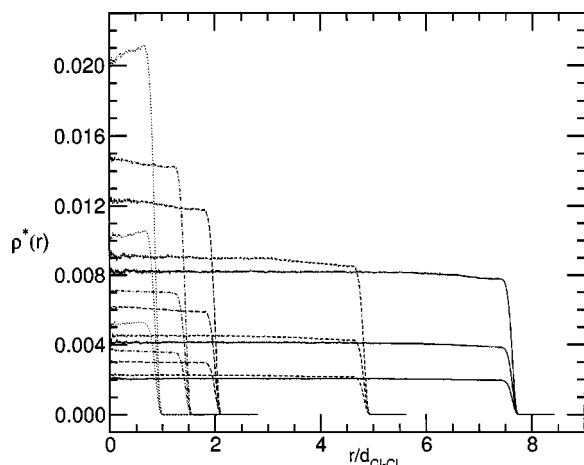

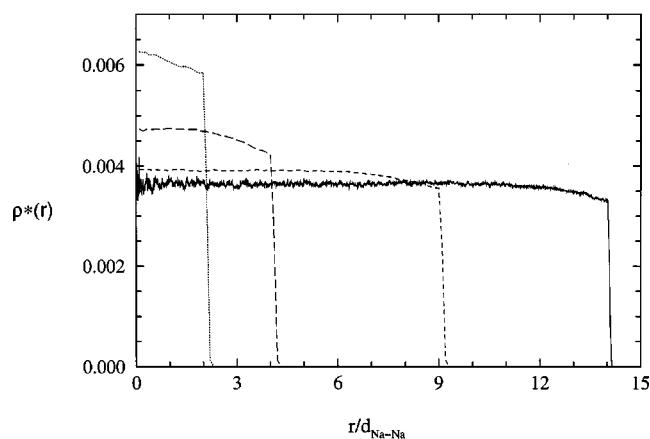FIG. 3. Same as Fig. 2, but for continuum solvent RPM: (Cl$^+$,Cl$^-$).

FIG. 4. Ionic density function $\rho^*_{Na}(r)=[N_{Na^+}(r)$ $+N_{Na^-}(r)]d^3_{Na\text{-}Na}/V$, r being the radial distance from the cylindrical axis, for continuum solvent RPM:(Na$^+$,Na$^-$) at $c_{Na}=0.1M$ obtained as described in Refs. [25,38]. Notation used is as follows: solid line, $R=15d_{Na\text{-}Na}$; short-dashed line, $R=10d_{Na\text{-}Na}$; long-dashed line R $=5d_{Na\text{-}Na}$; dotted line, $R=3d_{Na\text{-}Na}$.

tance toward the wall. For a lower $c_\lambda<0.1M$, $\rho^*(r)$ varies almost uniformly with the radial distance across the channel. The structure of $\rho^*(r)$ at $c_\lambda=0.1M$ is consistent with our previous RPM sodium simulation. To show this, we depict in Fig. 4 the $\rho^*(r)$ at $c_{Na}=0.1M$ obtained using a different set of Lennard-Jones energy and distance parameters [25]. These $\rho^*(r)$ compare favorably with those given in Fig. 2. The second feature has something to do with the effect of soft wall. In our model this repulsive force gives rise to an excluded volume, resulting in the physical volume available to cations and anions different from the actual simulation cell. Such a confinement has the consequence of restricting the centers of ions to lie within a region with an effective radius $R'=R$ $-\gamma d_{\lambda\mu}$ where γ is a "space-excluding" parameter. In view of this space restriction the actual cell volume available to ions is $\pi R'^2 H$. $\pi R'^2$ is thus the cross-sectional area to be used below for estimating the electric current density. In connection to this geometrical consideration, there is one further remark that we should comment on. In the present MD simulations, the smallest channel radius selected is 8.19 Å (equal $3d_{NaNa}$ or $1.69d_{ClCl}$). The nominal diameter of the cylinder less of the excluded region (estimated in conjunction with Table IV) is 10.38 (11.76) Å for the Cl$^-$ (Na$^+$). This effective channel diameter is larger than any of the characteristic minimum length scales (i.e., twice $d_{\lambda\mu}$ given in Table I) so that an ion (cation or anion) in our model electrolyte can easily pass another (cation or anion) without overlap (similar to the case of adsorbate Ne in Fig. 1(b) of Sholl and Fichthorn [6]). The implication is that neither sodium nor chlorine ions will show the single-file diffusion.

We now discuss the EMD simulation for D. Before presenting the results, we should make a remark on the numerical procedure used in the simulation. We run for $4\times10^7\tau^*$ after an equilibration run of $2\times10^6\tau^*$ for the RPM cases (Na$^+$,Na$^-$) and (Cl$^+$,Cl$^-$) and also the PM case (Na$^+$,Cl$^-$). The total number of particles, N (anions plus cations), used is 228. Also, we obtain D in each EMD by averaging the mean-square displacement run over at least 20 different time ori-
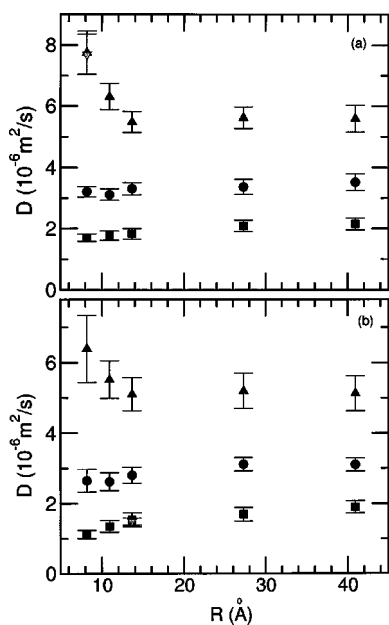
FIG. 5. (a) Diffusion coefficient constant D vs pore radius R at $c_{Na}=0.1M$ (bottom, solid squares), $0.05M$ (middle, solid circles), and $0.025M$ (top, solid up triangles) for continuum solvent RPM: (Na^+, Na^-). D is the average of D_{Na^+} and D_{Na^-}. The D for taking 30 origins is shown as the down triangle simulated for $R=8.19$ Å at $c_{Na}=0.025M$. (b) Diffusion coefficient constant D vs pore radius R at $c_{Na}=N_{Na^+}/V=0.1M$ (bottom, solid squares), $0.05M$ (middle, solid circles), and $0.025M$ (top, solid up triangles) for cations sodium in continuum solvent PM:(Na^+, Cl^-). Note that we have tested the simulation result at $c_{Na}=0.1M$ using the mass $m=0.058$ kg/mol (solid square) and $m=0.029$ kg/mol (down triangle) for the case $R=13.65$ Å.
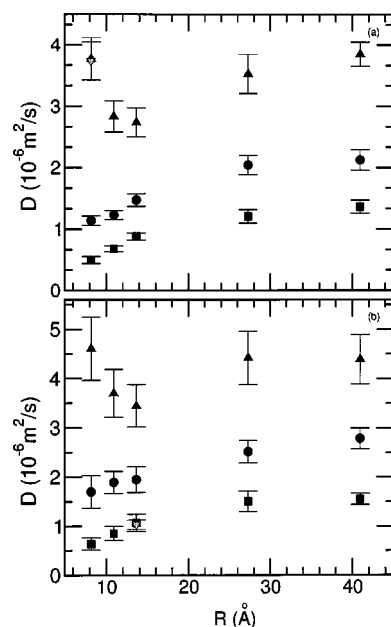

FIG. 6. (a) Diffusion coefficient constant D vs pore radius R at $c_{Cl}=0.1M$ (bottom, solid squares), $0.05M$ (middle, solid circles), and $0.025M$ (top, solid up triangles) for continuum solvent RPM:(Cl^+, Cl^-). D is the average of D_{Cl^+} and D_{Cl^-}. The D for taking 30 origins is shown as the down triangle simulated at $c_{Cl}=0.025M$ and for $R=8.19$ Å. (b) Diffusion coefficient constant D vs pore radius R at $c_{Cl}=N_{Cl^-}/V=0.1M$ (bottom, solid squares), $0.05M$ (middle, solid circles), and $0.025M$ (top, solid up triangles) for anions chlorine in continuum solvent PM:(Na^+, Cl^-). Note that we have tested the simulation result at $c_{Cl}=0.1M$ using the mass $m=0.058$ kg/mol (solid square) and 0.029 kg/mol (down triangle) for the case $R=13.65$ Å.

gins. We check carefully that this value for D is sufficient, since averaging D greater than 20 different time origins gives little change (see Figs. 5 and 6 each for a case study). Note that D for the RPM case was determined by taking the average values of $D_{\lambda+}$ and $D_{\lambda-}$ whereas for the PM case D_{Na^+} and D_{Cl^-} were calculated separately. Figures 5(a) and 6(a) depict the results of D vs R for the RPM:(Na^+, Na^-) and RPM: (Cl^+, Cl^-), respectively, and in the same figures we compare separately with D_{Na^+} [Fig. 5(b)] and D_{Cl^-} [Fig. 6(b)] extracted from the PM:(Na^+, Cl^-). As for $\rho^*(r)$, we consider in each case three ionic concentrations c_λ ($\lambda=$Na or Cl): namely, $0.025M$, $0.05M$ and $0.1M$. There are three aspects of the simulations that merit emphasis. First, for the RPM:(Na^+, Na^-), the diffusion coefficient constant at $c_{Na}=0.1M$ increases with increasing (or decreases with decreasing) R, achieves the value $D_{Na}\approx 2.08\times 10^{-6}$ m^2/s at $R=27.3$ Å ($10d_{Na-Na}$) and approaches $D_{Na}\approx 2.15\times 10^{-6}$ m^2/s for $R>27.3$ Å. A spectacular behavior in D_{Na} is that it remains almost independent of R at $c_{Na}=0.05M$ but at $c_{Na}=0.025M$, D_{Na} increases anomalously with radial distance $R\lesssim 13.65$ Å Second, for the RPM:(Cl^+, Cl^-), the general trend of D_{Cl} with c_{Cl} as a function of R mimics closely the results for the RPM sodium. Here the change of D_{Cl} vs R behaves in the usual manner at $c_{Cl}=0.1M$ and $0.05M$; that is, the magnitude of D_{Cl} decreases with decreasing R. However, at $c_{Cl}=0.025M$, an anomalous increase in D_{Cl} is again pre-

dicted for $R<13.65$ Å ($R=2.81d_{Cl-Cl}$). In other words, the concentration c_{Cl} at which D is independent of R for the RPM:(Cl^+, Cl^-) is slightly lower, falling into a value that lies somewhere between $0.025M$ and $0.05M$. Third, D_{Na} or D_{Cl} vs R for PM: (Na^+, Cl^-) generally follows the same pattern as the D data in the RPM, but the magnitude of D_{Na} (D_{Cl}) decreases (increases) with respect to the RPM.

The first aspect can be interpreted by resorting to two factors: one factor is the electrostatic interactions among cations, anions and between the two species (energetic factor), and the other factor is the interactions between the ions and the confining wall (entropic factor). At $c_{Na}=0.1M$, the former is presumably dominant since at higher concentrations there is a tendency for the ions within small R to be more structured (Figs. 2 and 3) and the entropy is therefore decreased. It appears that the ion-wall interactions at $c_{Na}=0.1M$ would lead to more structuring and this kind of ordering would lead to a decrease in D as R is reduced. As c_{Na} is reduced, we find the Coulombic interactions among cations, anions as well as between them weakened; the repulsive ion-wall interactions, on the other hand, begin to play a more active role in contributing to the Coulombic forces felt by ions (Table III). This happens in the following manner. As an ith cation or anion at r_i moves into the region $r_i \geq r_{min}(\lambda w)$ [defined by Eq. (6)], the ion-wall force operates and moves it radially inward to a new position. The tagged ion at r_i thus interacts

TABLE III. Number of cations, $N_{\lambda+}$ plus anions, $N_{\lambda-}$ (λ=Na or Cl), out of a total number of 228 ions that fall into the ion-wall interaction region $[r \geqslant r_{\min}(\lambda,w)]$ as a function of the cylindrical radius R for c_λ=0.1M, 0.05M, and 0.025M. The $r_{\min}(\lambda,w)$=R $-1.006 d_{\text{Na-Na}}$ (or $R-1.023 d_{\text{Cl-Cl}}$) is the minimum distance defined by Eq. (6). The ion-wall interacting number is calculated by the formula: $228\Sigma_{r \geqslant r_{\min}(\lambda,w)} \rho^*(r)\Delta r_i / \Sigma_i \rho^*(r)\Delta r_i$ where $\rho^*(r)=[N_\lambda +(r)+N_\lambda-(r)]d_{\lambda\lambda}^3/V$ is the reduced radial density of $(N_{\lambda+}+N_{\lambda-})$ ions.

RPM	R (Å)/c_λ	0.1M	0.05M	0.025M
	8.19	15	15	15
	10.92	10	10	10
(Na$^+$,Na$^-$)	13.65	8	8	8
	23.7	4	4	4
	40.95	2	2	2
	8.19	53	54	52
	10.92	31	30	30
(Cl$^+$,Cl$^-$)	13.65	21	21	21
	23.7	9	9	9
	40.95	6	6	6

electrostatically with all other ions preferentially those with an opposite polarity. The resulting configuration (an entropic factor) from which the system evolves subsequently must be different from the bulk environment where the influence of confined geometry is absent. Our results of simulations show that such ion-wall interactions increase with decreasing R for all of c_λ (see Table III for numerical evidence). The consequence is that the entropy of the system of cations and anions is enhanced for a smaller R. This scenario can be seen from Figs. 2 and 3 where $\rho^*(r)$ varies *uniformly* for c_λ=0.025M and nonuniformly (or linearly) for c_λ=0.1M. The electrostatic interaction depends on the average distance between ions. For a smaller pore radius, the smaller cross-sectional area leads to a decrease in density in the axial dimension and thus increases the ion-ion distance. This, in general, would lower the electrostatic interaction and is more pronounced at a lower concentration. In fact, the present simulation predicts that D_λ increases anomalously for $c_{\text{Na}}<0.05M$ and $R<13.65$ Å in the RPM:(Na$^+$,Na$^-$) or $c_{\text{Cl}}<0.05M$ and $R \lesssim 19.44$ Å in the RPM:(Cl$^+$,Cl$^-$); these behaviors for D$_\lambda$, shown in Figs. 7(a) and 8(a) for the RPM and in Figs. 7(b) and 8(b) for the PM, clearly manifest the response of ions in confined space. Coming to the second aspect, this can be explained by the inertia effect and the relatively larger physical size of chlorine. Both properties slow down the motion, but they do not change the basic (Coulomb) interactions among anions, cations, and between them and the wall. In view of the normal behavior of D_λ at c_λ=0.1M where it *decreases* with *reducing* R and the abnormal behavior at $c_\lambda<0.05M$ where D_λ *increases* with *reducing* R, we would anticipate the existence of a threshold c_λ at which concentration D_λ is independent of R. When this happens the electrostatic interaction (energetic factor) will just balance the ion-wall interaction (entropic factor). Finally, the third aspect can
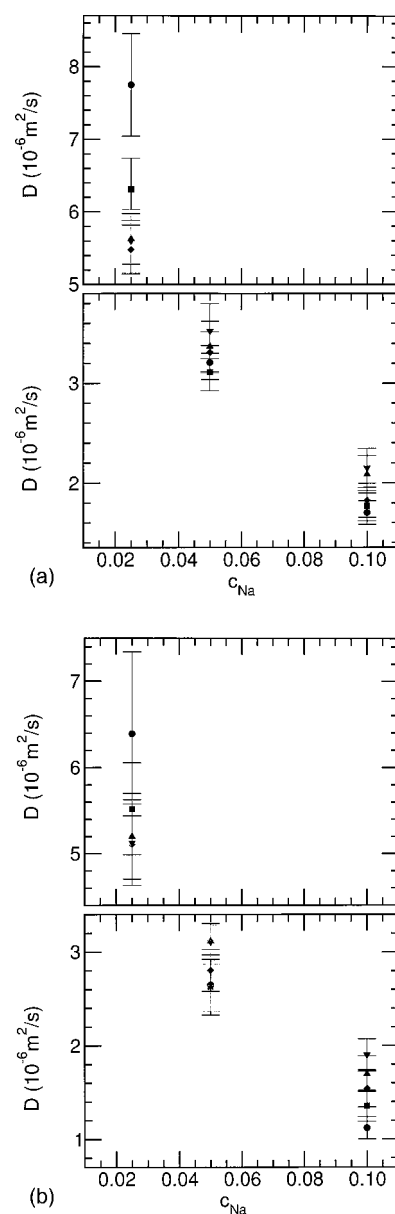

FIG. 7. (a) Diffusion coefficient constant D vs concentration c_{Na} for continuum solvent RPM:(Na$^+$,Na$^-$). Notation used is as follows: down triangle, R=40.95 Å; up triangle, R=27.3 Å; diamond, R =13.65 Å; square, R=10.92 Å; circle, R=8.19 Å. Note that the upper figure is for c_{Na}=0.025M enlarged for clarity and separated from cases for c_{Na}=0.05M and 0.1M given in the lower figure. (b) Same as (a), but for Na$^+$ in continuum solvent PM:(Na$^+$,Cl$^-$).

be understood by noticing that the larger anions Cl$^-$ in the PM have less room to wander about compared with the smaller anions Na$^-$ in the RPM. The opposite situation occurs to cations in the PM (compared with the RPM case) where, now, more space is available to Na$^+$ ions instead of Cl$^+$ cations in the RPM. The entropic factor is therefore one of the reasons for the decrement (increment) in magnitude of D_{Na} (D_{Cl}). The ionic radial density functions given in Figs. 9(a) and 9(b), respectively, for Na$^+$ and Cl$^-$ in the model electrolyte CSPM further illustrate our proposition.
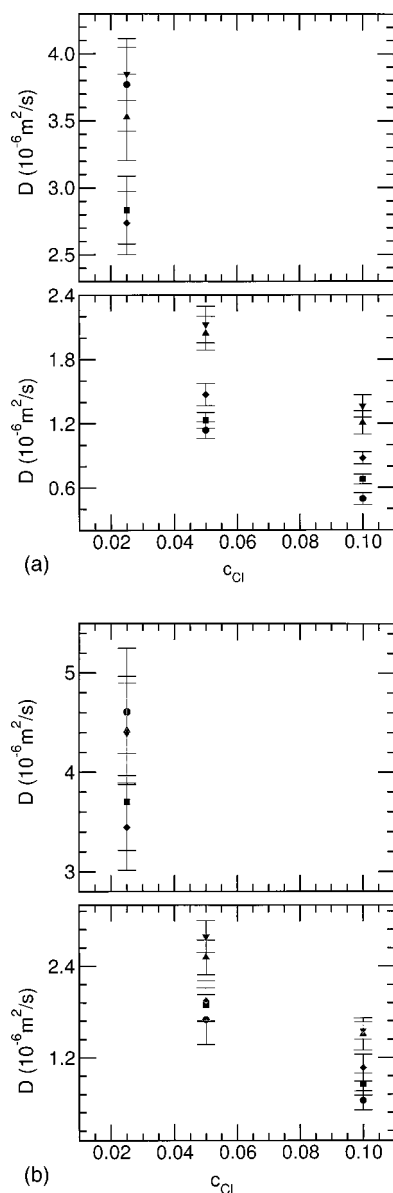
FIG. 8. (a) Same as Fig. 7(a), but for continuum solvent RPM:(Cl$^+$,Cl$^-$). (b) Same as Fig. 7(a), but for Cl$^-$ in continuum solvent PM:(Na$^+$,Cl$^-$).

FIG. 9. (a) Ionic density function for cations $\rho_{\mathrm{Na}}^*(r)$ $=N_{\mathrm{Na}^+}(r)d_{\mathrm{Na\text{-}Na}}^3/V$, r being the radial distance from the cylindrical axis, for continuum solvent PM:(Na$^+$,Cl$^-$) calculated by taking the time average of $2\times10^7\tau^*$ for $R/d_{\mathrm{Na\text{-}Na}}=3$ (dotted line), 4 (dot-dashed line), 5 (long-dashed line), 10 (short-dashed line), and 15 (solid line) at $c_{\mathrm{Na}}=0.1M$ (top), $0.05M$ (middle), and $0.025M$ (bottom). The total number of anions and cations is 228 and $d_{\mathrm{Na\text{-}Cl}}$ $=3.87$ Å (b) Same as (a), but for anions.

B. Self-diffusion coefficient: Discrete solvent primitive model

Before describing the general characteristics of the DSPM, it may be helpful to recall a relevant work of Lynden-Bell and Rasaiah [20] who reported a similar MD simulation for a system comprising of one solute embedded in point-charge SPC/E solvent molecules. Preparing the single ion (Na$^+$ or Cl$^-$) and the water molecules in an infinitely long cylindrical pore with smooth repulsive walls, Lynden-Bell and Rasaiah studied the radial density distribution of ion (Na$^+$ or Cl$^-$) and solvent molecules as well as the diffusion coefficient of the isolated ion as a function of pore radius. They noticed that the smaller Na$^+$ ion tends to occupy the center of the cylinder while the larger Cl$^-$ ion is more likely found near the wall. Lynden-Bell and Rasaiah attributed such a difference in the distributions of positive and
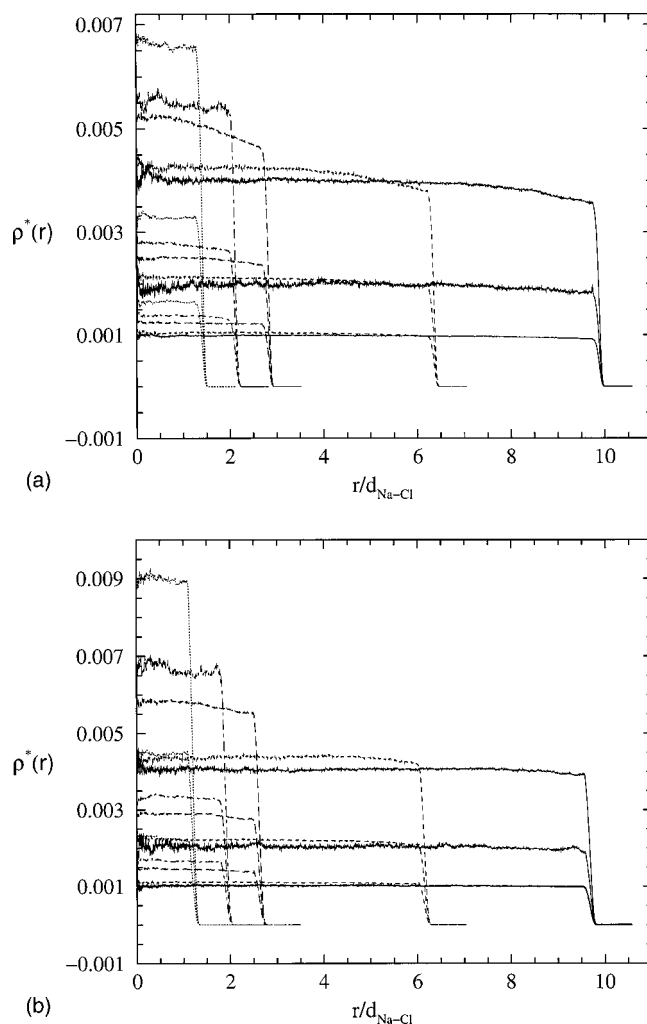
negative ions to the entropic factor. Since the potential parameters used here (Table I) and by them are essentially the same (except for $\sigma_{\mathrm{Cl\text{-}O}}=3.785$ Å, a different form of the ion-wall repulsive potential and the treatment of water molecules as point charges), the general behavior presented there for the single-ion properties is a useful contrast to the collective diffusion given here, at least qualitatively.

We now proceed to study the general properties of the DSPM and compare it with the CSPM. Let us first look at the density distribution of ions. For this purpose, we perform a simulation for the DSPM for a total number (Na$^+$+Cl$^-$) of 76 ions dispersed in 29 666 water molecules modeled in this work by neutral soft cores. The solvent volume fraction is estimated to be $\eta_s=0.2$. Figures 10(a)–10(c) display the radial density profiles of ions prepared at the concentration $c_\lambda=0.025M$ for the cylindrical radii $R=8.19$, 13.65, and 27.3 Å, respectively. In contrast to the density profiles of
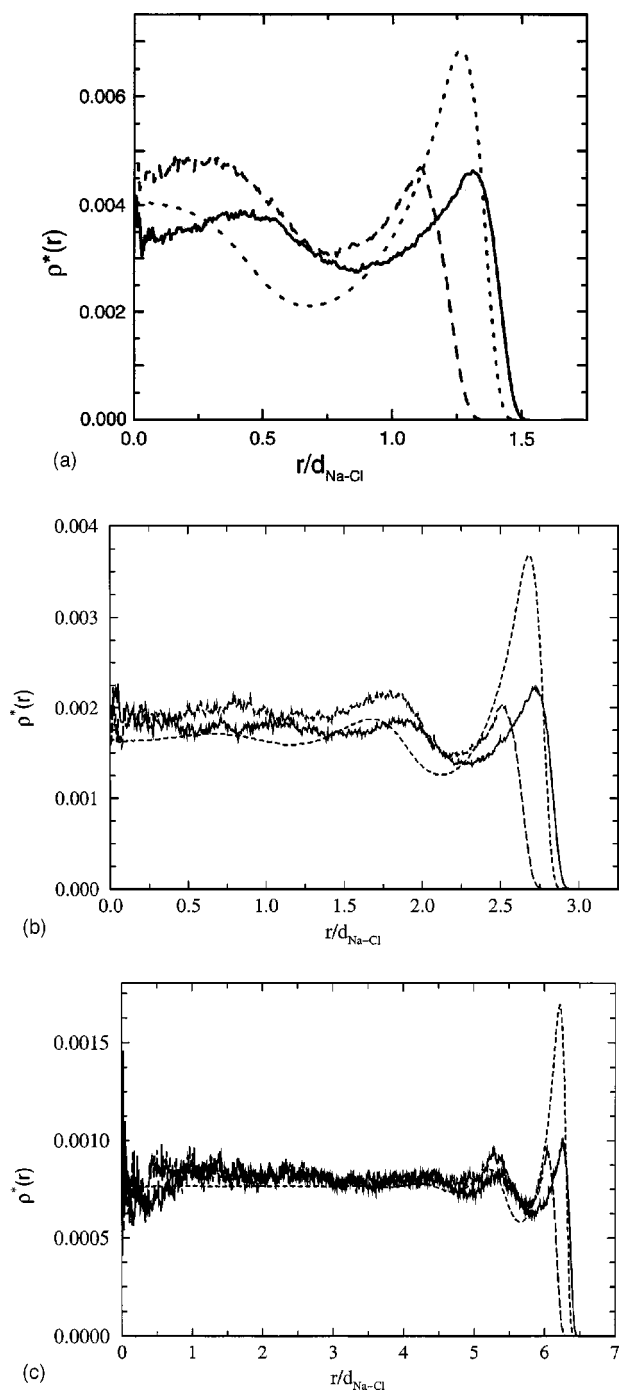
FIG. 10. (a) Ionic radial density functions ρ_{Na}^{*} $(r)=N_{Na^{+}}(r)d_{Na\text{-}Na}^{3}/V$, $\rho_{Cl}^{*}(r)=N_{Cl^{-}}(r)d_{Cl\text{-}Cl}^{3}/V$, and $\rho_{s}^{*}(r)$ $=N_{s}(r)d_{Na\text{-}Cl}^{3}/V$, r being the radial distance from the cylindrical axis, for Na^{+} (solid line) in discrete solvent PM:(Na^{+},Cl^{-}), Cl^{-} (long-dashed line) in discrete solvent PM:(Na^{+},Cl^{-}), and water (short-dashed line), respectively. The number of ions used is $N_{Na^{+}}(r)+N_{Cl^{-}}(r)=76$ for ions and $N_{s}=29\,666$ for solvent. The discrete solvent volume fraction is estimated to be $\eta_{s}=0.2$. The simulation was carried out with $1\times10^{6}\tau^{*}$ equilibration time and run further for $1\times10^{7}\tau^{*}$ taking an average of five time origins. The concentration of ions and the pore radius R are 0.025M and 8.19 Å, respectively. (b) Same as (a), but for radius $R=13.65$ Å. (c) Same as (a), but for radius $R=27.3$ Å.

TABLE IV. Comparison of the excluded space induced by ion-wall interaction for the DSPM (upper two rows) and CSPM) (lower two rows) for Na^{+} and Cl^{-} at concentration 0.025M for different pore radii. Numerical values given are distances (in units of Å) measured from the wall.

Ion	R (Å)		
	8.19	13.65	27.3
Na^{+}	2.31	2.25	2.20
Cl^{-}	3.00	2.95	2.90
Na^{+}	2.35	2.35	2.30
Cl^{-}	3.04	3.05	3.00

Lynden-Bell and Rasaiah (Fig. 9 in Ref. [20]), the radial density distribution functions of Na^{+} and Cl^{-} are reversed with the ions of Na^{+} (Cl^{-}) distributed closer (farther) from the pore center while those of water molecules prefer to stay near the wall. Note that the number of water molecules used in the present simulation is significantly larger. In comparison with the CSPM, the DSPM radial density functions exhibit structures that are entirely different. The most obvious disparity is the accumulation of ions in the vicinity of the wall. For the DSPM, the density distribution functions of ions display two clear peaks which are located, for pore radius $R=8.19$ Å, at $r_{Na^{+}}\approx5.11$ and 1.66 Å for cations and at $r_{Cl^{-}}\approx4.30$ and 0.89 Å for anions; for $R=13.65$ Å, at $r_{Na^{+}}\approx10.53$ and 7.16 Å and $r_{Cl^{-}}\approx9.71$ and 6.97 Å; and for $R=27.3$ Å, at $r_{Na^{+}}\approx24.2$ and 20.8 Å and $r_{Cl^{-}}\approx23.4$ and 20.4 Å, and they oscillate into the center of the cylinder. The oscillatory profile is relatively stronger in the region near the cylindrical axis for $R=8.19$ Å compared with those for $R=13.65$ and 27.3 Å. In fact, the $\rho^{*}(r)$ in the two larger pore radii approach the cylindrical axis with nearly constant density. The regions where the ions are excluded by the ion-wall interaction are given in Table IV in which are included for comparison the corresponding data in the CSPM. Also, it is seen that the $\rho^{*}(r)$ of solvent particles peaks at positions $r_{water}\approx4.91$, 10.37, and 24.0 Å, respectively, for pore radii $R=8.19$, 13.65, and 27.3 Å, closer to the wall, but lies generally in between those $\rho^{*}(r)$ of cations and anions. This behavior differs from the simulated $\rho^{*}(r)$ using the DSRPM [13] and may be attributed to the more realistic DSPM considered in the present simulation work and to the fact that the concentration of electrolyte is lower than that of Tang *et al.* [13] ($c_{\lambda}=0.1M$). Now, according to the works of Tang *et al.* [13] and others [41–43] a localized distribution of ions would lead to a lower value of the local diffusion coefficient, and naturally, the pore-averaged D_{λ} will also be lower. For instance, our simulated D_{λ} data at channel radius $R=13.65$ Å for the DSPM yield $D_{Na^{+}}=0.0737\pm0.005\,26\times10^{-6}$ m^{2}/s and $D_{Cl^{-}}=0.049\,46\pm0.003\,13\times10^{-6}$ m^{2}/s; these values are indeed much smaller in magnitude compared with those of the CSPM ($D_{Na^{+}}=5.107\,12\pm0.470\,99\times10^{-6}$ m^{2}/s and $D_{Cl^{-}}=3.445\,07\pm0.4308\times10^{-6}$ m^{2}/s). The decrease in D_{λ} is the result of the effect of discrete solvent molecules.

C. Conductivity: Continuum solvent primitive model

In view of the anomalous behavior of D at $c_\lambda = 0.025M$, we now present our NEMD results for σ^* in the CSPM. Figures 11(a)–11(c) display plots of $\sigma^*_{Na^+}$ in electrolyte NaCl $\sigma^*_{Cl^-}$ in electrolyte NaCl, and total $\sigma^* = \sigma^*_{Na^+} + \sigma^*_{Cl^-}$ of electrolyte NaCl at $c_\lambda = 0.025M$, respectively. Separately, we included in each plot (a) σ_λ or σ^* vs E^*_z simulated for different R and (b) σ_λ or σ^* vs R for the equilibrium case obtained by extrapolating $E^*_z \to 0$. As can be seen from these figures, the linear response behavior is satisfied generally in all cases considered here. Let us summarize three specific features. First, the $\sigma^*_{Na^+}$ and $\sigma^*_{Cl^-}$ at the large pore radius $R = 27.3$ Å have nearly constant magnitudes or weakly increase with increasing E^*_z resulting in the total σ^* increases with increasing E^*_z. As R decreases to 13.65 Å, σ^* of either cations or anions is in opposition to the change in E^*_z. Thus the $\sigma^*_{Na^+}$, $\sigma^*_{Cl^-}$ and σ^* all decrease with increasing E^*_z as the pore radius becomes small (in the present case $R \lesssim 27.3$ Å). This trend differs from the simulation work of Tang *et al.* [25] at $c_{Na} = 0.1M$ where there they predicted the RPM: (Na^+, Na^-) σ^* increases with increasing E^*_z at $R = 10 d_{Na-Na}$ and $5 d_{Na-Na}$, but reversing behavior is observed at $R = 3 d_{Na-Na}$. Second, the simulated $\sigma^*_{Na^+}$, $\sigma^*_{Cl^-}$ and σ^* all show an anomalous increment as the channel radius is decreased. Third, for although the electric conductivity of sodium ions at $R = 27.3$ ($\sigma^*_{Na^+} = 0.008\ 36$) and 13.65 Å ($\sigma^*_{Na^+} = 0.019$) is larger than $\sigma^*_{Cl^-}$ at the same R ($\sigma^*_{Cl^-} = 0.006\ 22$ and $0.014\ 83$, respectively), the electric conductivity $\sigma^*_{Cl^-} = 0.026\ 76 \approx \sigma^*_{Na^+} = 0.026\ 82$ is observed at $R = 8.19$ Å. The first two features qualitatively correlate with the results of D vs R given in Figs. 5 and 6. Quantitatively, the trend is similar to our preceding work for RPM results at $c_\lambda = 0.1M$ (Fig. 7 in Ref. [13]) in that it is slightly different from the D_λ of ions obtained within the context of the Nernst-Einstein equation. This would point to the general validity of the Nernst-Einstein equation for confined electrolytes such as the CSPM reported here. The third feature, however, needs further explanation. Returning to Figs. 9(a) and 9(b) for the radial density functions, we observe an unusual feature. At $c_\lambda = 0.025M$, $\rho^*(r)$ is uniform as a function of r and its magnitude increases with decreasing R. Both cations and anions separately follow this trend. There is, however, one basic difference. At $R = 8.19$ Å, $\rho^*_{Na^+}(r) \approx 0.001\ 65$ and is much less than $\rho^*_{Cl^-}(r) \approx 0.002\ 25$ at the same R. The difference is certainly larger compared with those at $R = 13.65$ $[\rho^*_{Na^+}(r) \approx 0.001\ 25, \rho^*_{Cl^-}(r) \approx 0.0014]$ and 27.3 Å $[\rho^*_{Na^+}(r) \approx 0.001\ 05, \rho^*_{Cl^-}(r) \approx 0.0011]$. In other words, the average cross-sectional density of anions at $R = 8.19$ Å is higher (see also Table III) than that of cations. As a consequence, the average axial density of anions is generally lower, implying that the anion-anion distance in the axial direction, on the average, will be larger. It is therefore quite plausible that $\sigma^*_{Cl^-}$ at a smaller R can achieve a value comparable to $\sigma^*_{Na^+}$. In our preceding work [13], the NEMD simulation for severely confined systems with $R = 1.5$ and $2 d_{Na-Na}$ showed that σ^* decreases rapidly to zero. We believe that a similar phenomenon will possibly be observed also for the CSPM.
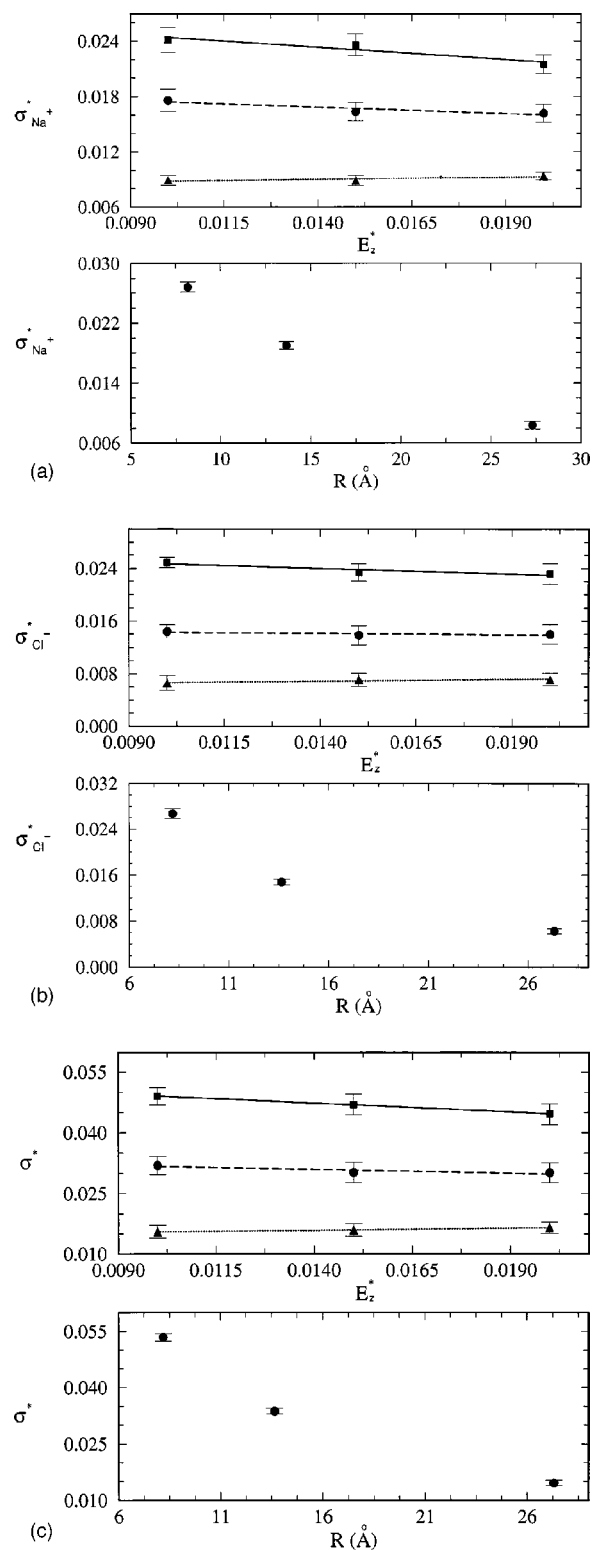

FIG. 11. (a) Reduced electric conductivity σ^* vs applied uniform electric field E^*_z (upper figure) for cations Na^+ in continuum solvent PM: (Na^+, Cl^-) simulated at $c_{Na} = 0.025M$ for channel radii $R = 8.19$ (squares), 13.65 (circles), and 27.3 (triangles) Å. The lower figure depicting σ^* vs R (Å) is obtained by extrapolating $E^*_z \to 0$ corresponding to the equilibrium situation. (b) Same as (a), but for anions Cl^- in continuum solvent PM: (Na^+, Cl^-). (c) Same as (a) but for the $Na^+ + Cl^-$ system in continuum solvent PM: (Na^+, Cl^-).

IV. SUMMARY AND CONCLUSION

The EMD and NEMD simulations were performed to study the equilibrium and nonequilibrium properties of a model electrolyte NaCl which is prepared at three electrolytic concentrations—namely, $c_\lambda = 0.1M$, $0.05M$, and $0.025M$—and is confined to an infinitely long, uncharged cylindrical pore. For the EMD simulations, we compare the continuum solvent RPM and PM for the diffusion coefficient as a function of the radius of the cylinder at each ionic concentration. Our simulation results show that it decreases with reducing R at $c_\lambda = 0.1M$, shows a weak dependence on R at $c_\lambda = 0.05M$, and as c_λ falls down to $0.025M$, D decreases initially with R (from $15d_{\lambda\mu}$ to approximately $5d_{Na-Na}$ or $2.81d_{Cl-Cl}$) and then increases anomalously with further reducing R. Both continuum solvent RPM and PM display these interesting features. The mechanism behind the anomalous change of D with R for different c_λ can be understood qualitatively in this work by looking closely at the Coulombic interactions (energetic factor) between anions and cations and at the role played by the wall in pushing away those ions that "invade" the repulsive region $r \geq r_{\lambda w}(\min)$, thereby changing the ionic configuration (entropic factor), which in turn alters the electrostatic coupling among ions. For the NEMD simulations, the simulated electric conductivity at the same $c_\lambda = 0.025M$ for different R follows the same anomalous pattern as D vs R. In contrast to the CSPM, the diffusion coefficient for the DSPM under the condition of same R and c_λ behaves differently due to increased interactions between ions and solvent molecules. Here, in addition to ions, the solvent molecules interact also with the wall. Since the number of water molecules is significant, an immediate consequence is that the solvent-wall interactions may easily overwhelm the ion-wall interactions. The behavior of D is therefore very much influenced by interactions between the ions and the solvent molecules. Normal diffusive motion for the anions and the cations with decreasing R at different c_λ is thus to be anticipated.

[1] D. A. Doyle, J. M. Cabral, R. A. Pfuetzner, A. Kuo, J. M. Gulbis, S. L. Cohen, B. T. Chait, and R. MacKinnon, Science **280**, 69 (1998).

[2] B. Roux and M. Karplus, Annu. Rev. Biophys. Biomol. Struct. **23**, 731 (1994).

[3] L. R. Forrest and M. S. Sansom Curr. Opin. Struct. Biol. **10**, 174 (2000).

[4] D. Keffer, A. V. Mccormick, and H. T. Davis, Mol. Phys. **87**, 367 (1996).

[5] K. Hahn, J. Kärger, and V. Kukla, Phys. Rev. Lett. **76**, 2762 (1996).

[6] D. S. Sholl and K. A. Fichthorn, J. Chem. Phys. **107**, 4384 (1997).

[7] T. Chou and D. Lohse, Phys. Rev. Lett. **82**, 3552 (1999).

[8] S. Rivera and T. S. Sorenson, Mol. Simul. **13**, 115 (1994).

[9] M. Lee and K. Y. Chan, Chem. Phys. Lett. **275**, 56 (1997).

[10] D. Boda, D. D. Busath, D.Henderson, and S. Sokolowski, J. Phys. Chem. B **104**, 8903 (2000).

[11] B. Hribar, V. Vlachy, L. B. Bhuiyan, and C. W. Outhwaite, J. Phys. Chem. B **104**, 11 522 (2000).

[12] M. Lee, K. Y. Chan, D. Nicholson, and S. Zara, Chem. Phys. Lett. **307**, 89 (2000).

[13] Y. W. Tang, I. Szalai, and K. Y. Chan, J. Phys. Chem. A **105**, 9616 (2001).

[14] V. Vlachy and A. D. J. Haymet, J. Electroanal. Chem. Interfacial Electrochem. **283**, 77 (1990).

[15] A. Steck and H. L. Yeager, J. Electrochem. Soc. **130**, 1297 (1983).

[16] C. Gavach, G. Pamboutzoglou, M. Nedyalkov, and G. Poucelly, J. Membr. Sci. **45**, 37 (1989).

[17] G. B. Westermann-Clark and J. L. Anderson, J. Electrochem. Soc. **130**, 839 (1983).

[18] P. K. Hansma, B. Drake, O. Marti, S. A. C. Gould, and C. B. Prater, Science **243**, 641 (1989).

[19] B. Sackmann and E. Neher, *Single Channel Recording* (Plenum, New York, 1995).

[20] R. M. Lynden-Bell and J. C. Rasaiah, J. Chem. Phys. **105**, 9266 (1996).

[21] G. R. Smith and M. S. P. Sansom, Biophys. J. **73**, 1364 (1997).

[22] R. S. Eisenberg, Acc. Chem. Res. **31**, 117 (1998).

[23] W. Nernst, Z. Phys. Chem., Stoechiom. Verwandtschaftsl. **2**, 613 (1888); **4**, 129 (1889).

[24] M. Planck, Annu. Rev. Phys. Chem. **39**, 161 (1890).

[25] Y. W. Tang, I. Szalai, and K. Y. Chan, Mol. Phys. **99**, 309 (2001).

[26] S. S. Nivarthi, A. V. McCormick, and H. T. Davis, Chem. Phys. Lett. **229**, 297 (1994).

[27] V. Gupta, S. S. Nivarthi, A. V. McCormick, and H. T. Davis, Chem. Phys. Lett. **247**, 596 (1996).

[28] V. Kukla, J. Kornatorwski, D. Demuth, I. Girnus, H. Pfeifer, L. V. C. Rees, S. Schunk, K. K. Unger, and J. Kärger, Science **272**, 702 (1996).

[29] G. J. Tjatjopoulos, D. L. Feke, and J. A. Mann, J. Phys. Chem. **92**, 4006 (1988).

[30] E. Spohr, Electrochim. Acta **44**, 1697 (1999).

[31] P. S. Crozier, D. Henderson, R. L. Rowley, and D. D. Busath, Biophys. J. **81**, 3077 (2001).

[32] M. P. Allen and D. J. Tildesley, *Computer Simulations of Liquids* (Clarendon, Oxford, 1987), p. 21.

[33] D. M. Heyes, *The Liquid State (Application of Molecular Simulation)* (John Wiley & Sons, Chichester, 1997).

[34] J. M. D. MacElroy and S. H. Suh, Mol. Phys. **60**, 475 (1987).

[35] D. M. Heyes, Phys. Rev. B **37**, 5677 (1988).

[36] D. C. Rapaport, *The Art of Molecular Dynamics Simulation* (Cambridge University Press, London, 1995).

[37] G. S. Heffelfinger and F. van Swol, J. Chem. Phys. **100**, 7548 (1994).

[38] I. M. Svishchev and P. G. Kusalik, Physica A **192**, 628 (1993); Phys. Chem. Liq. **26**, 237 (1994).

[39] S. S. Sarman, D. J. Evans, and P. T. Cummings, Phys. Rep.

305, 1 (1998).

[40] D. J. Evans and G. P. Morriss, Comput. Phys. Rep. **1**, 297 (1984).

[41] H. T. Davis, J. Chem. Phys. **86**, 1474 (1987).

[42] T. K. Vanderlick and H. T. Davis, J. Chem. Phys. **87**, 1791 (1987).

[43] D. Henderson, *Fundamentals of Inhomogeneous Fluids* (Marcel Dekker, New York, 1992).